

## 基于连续小波变换的激光外差干涉非线性误差补偿

王煜, 陈洪芳\*

北京工业大学材料与制造学部北京市精密测控技术与仪器工程技术研究中心, 北京 100124

**摘要** 测量分辨率和精度的不断提高是激光外差干涉测量的发展趋势,而抑制激光外差干涉测量精度进一步提升的主要因素是周期性非线性误差。提出了一种基于连续小波变换的激光外差干涉非线性误差补偿方法。对非线性误差函数进行 Morlet 小波变换,利用小波系数矩阵信息提取小波脊线,分析小波脊线上的特征信息,重构一次谐波非线性误差;利用最小二乘非线性拟合方法迭代拟合出二次谐波非线性误差。实验结果表明,将此方法应用于激光外差干涉测量系统中,非线性误差分量由 5.97 nm 减小到 1.09 nm,非线性误差分量减小至原来的 18%。该方法可有效抑制非线性误差的影响,并提高激光外差干涉测量的精度。

**关键词** 测量;激光外差干涉;非线性误差;连续小波变换;最小二乘非线性拟合

**中图分类号** TH741

**文献标志码** A

**DOI:** 10.3788/CJL202249.2104006

## 1 引言

激光外差干涉技术利用载波技术将被测物理量的信息转换成调频或调相信号,光电探测器接收到的干涉信号是交流信号,具有信噪比高、抗干扰能力强、易于实现高分辨率和动态实时测量的优点。Quenelle<sup>[1]</sup>于 1983 年首次指出激光外差干涉测量中会出现周期性的非线性误差。激光外差干涉测量中的非线性误差主要是共光路的测量光和参考光无法完全分离而导致的频率和偏振混叠<sup>[2]</sup>。通过调整激光外差干涉光路结构,改善测量光和参考光的椭圆极化、非正交性等,可以减小非线性误差的影响。Guo 等<sup>[3]</sup>提出在激光器的出光端与分光镜之间放置一个相位补偿器,提高光束的正交性,能够有效抑制非线性误差。陈洪芳等<sup>[4-5]</sup>将角锥绕运动方向旋转一定角度以引入额外的相位进行补偿,非线性误差变为原来的 40%。Fu 等<sup>[6]</sup>在参考臂中加入衰减器,通过调节衰减器将非线性误差从 5.15 nm 降低到 0.24 nm。Lu 等<sup>[7]</sup>利用高消光比的偏振片,测量出激光偏振态和偏振分光镜透射系数等参数,实现了非线性误差的补偿。Yang 等<sup>[8-9]</sup>研制的双折射-塞曼双频激光干涉仪的非线性误差仅为 0.3 nm,比传统的塞曼双频激光干涉仪的非线性误差小一个数量级。

事实上,还可以通过处理参考信号和测量信号来实现非线性误差的补偿。Eom 等<sup>[10]</sup>提出了一种补偿非线性误差的椭圆拟合法,通过测量参考信号和测量信号拟合的椭圆参数,实现了非线性误差的补偿。为

了提高补偿效率,Eom 等<sup>[11]</sup>又提出通过校正参考信号和测量信号来正交性补偿非线性误差的方法。Wang 等<sup>[12]</sup>提出了一种卡尔曼滤波方法,有效实现了对非线性误差的实时补偿。严利平等<sup>[13]</sup>提出了一种基于卡尔曼滤波技术的 PGC-Arctan 解调算法,通过构建椭圆观测模型,实时获得相位载波生成的正交分量幅值和偏置的最优估计值,进而实现相位解调非线性误差的消除。此外,Lawall 等<sup>[14]</sup>提出了空间分离式激光干涉测量方法,从光源处分离双频激光束,避免了不同频率的激光发生频率混叠。Fu 等<sup>[15-17]</sup>提出了虚反射产生的非线性误差的补偿方法,将非线性误差分量减小到数十皮米量级。郝义伟等<sup>[18]</sup>提出非线性误差系数与信号光场有关,非线性误差系数是整个激光干涉测量系统在测量过程中的效果表征。Yu 等<sup>[19]</sup>提出了一种相位测量的单系数非线性误差补偿算法,对三维测量系统进行了补偿。

本文提出了一种激光外差干涉非线性误差补偿新方法,对非线性误差函数进行 Morlet 小波变换,重构了一次谐波非线性误差,利用最小二乘非线性拟合方法迭代拟合出二次谐波非线性误差,最终实现了非线性误差的抑制。

## 2 基于连续小波变换的非线性误差补偿

## 2.1 基于连续小波变换的一次谐波非线性误差补偿

在激光外差干涉系统中,可以将周期性非线性误差建模为纯正弦波的叠加,表示为

收稿日期: 2021-12-14; 修回日期: 2022-01-20; 录用日期: 2022-03-10

基金项目: 国家自然科学基金(52175491)

通信作者: \*chf0302@126.com

$$E_{\text{nonl}} = A_1 \sin[\theta_1(t)] + A_2 \sin[\theta_2(t)], \quad (1)$$

式中:  $t$  为时间;  $A_1$  和  $A_2$  分别表示一次谐波非线性误差和二次谐波非线性误差的振幅;  $\theta_1(t)$  和  $\theta_2(t)$  分别表示一次谐波非线性误差和二次谐波非线性误差的

相位。

Morlet 小波在分析信号方面具有强大的分辨多尺度功能,同时具有良好的局部化优势。本文所用的 Morlet 小波定义<sup>[20]</sup>为

$$\Psi f(u, s) = \frac{1}{\sqrt{s}} \int_{-\infty}^{+\infty} E_{\text{nonl}} \pi^{-\frac{1}{4}} \exp\left[\frac{j2\pi f_0(t-u)}{s}\right] \exp\left[-\frac{(t-u)^2}{2s^2}\right] dt, \quad (2)$$

式中:  $\Psi f(u, s)$  为连续小波变换系数,其中  $\Psi$  表示对函数进行小波变换,  $f(u, s)$  为周期性非线性误差函数;  $f_0$  为小波函数中心频率;  $u$  为时间因子;  $s$  为尺度因子,代表小波的周期尺度。

改变复 Morlet 小波的时间因子  $u$  和尺度因子  $s$  生成小波族,基于式(2)对式(1)的非线性误差函数进行连续小波变换,得到小波系数矩阵。小波系数矩阵中小波系数的模量  $a(u, s)$ 、相位  $\varphi(u, s)$  和小波脊线  $r(u)$  可分别表示为

$$a(u, s) = |\Psi f(u, s)|, \quad (3)$$

$$\varphi(u, s) = \arctan\left\{\frac{\text{Im}[\Psi f(u, s)]}{\text{Re}[\Psi f(u, s)]}\right\}, \quad (4)$$

$$r(u) = \max[|\Psi f(u, s)|], \quad (5)$$

式中:  $\text{Im}$  和  $\text{Re}$  分别表示小波系数的虚部和实部。

利用不同的时间参数、尺度参数和小波系数的模值可以构建一个三维曲面,曲面中的高点代表小波系数模值较大。小波系数模量越大,代表此处的时间参数和尺度参数构成的子小波与非线性误差曲线的相关性最好。连续小波变换的模值集中在脊线附近,脊线上分布的特征参数与非线性误差信号具有强的相关性。图 1 所示为 Morlet 小波变换之后得到的非线性误差曲线的小波系数模量图,其中小波模量越高代表在此位移和时间参数下的小波函数和非线性误差曲线的相关性越好。图 2 所示为提取后的小波脊线,滤除了冗余的小波系数,小波脊线的特性与非线性误差函数特性相近,分析小波脊线信息可以进一步得到非线性误差曲线的相关参数。

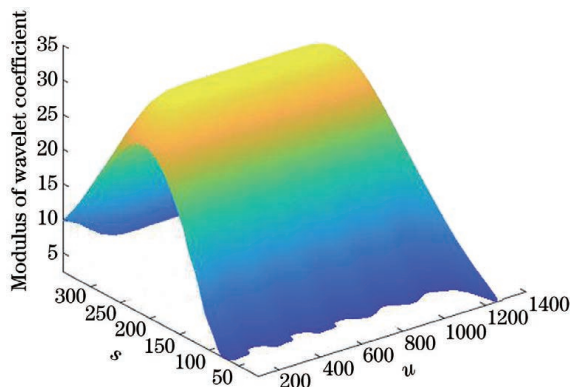


图 1 变换后的小波系数模量图

Fig. 1 Modulus diagram of wavelet coefficient after transformation

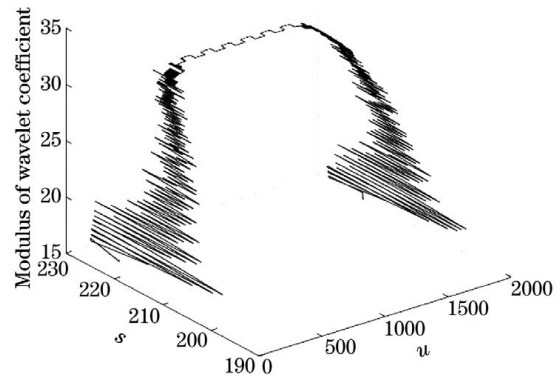


图 2 提取的小波脊线

Fig. 2 Extracted wavelet ridge

当脊线位置上的小波系数模量最大时,此处尺度  $s_1$  对应一次谐波非线性误差的频率,对应的相位为  $\varphi(u, s_1)$ 。单位振幅的一次谐波非线性误差表示为  $\sin[\varphi(u, s_1)]$ ,对应尺度  $s_2 = s_1/2$  的单位振幅的二次谐波非线性误差为  $\sin[2\varphi(u, s_1)]$ 。则非线性误差模型可以表示为

$$E_{\text{nonl}} = A_1 \sin[\varphi(u, s_1)] + A_2 \sin[2\varphi(u, s_2)]. \quad (6)$$

令不同尺度下测量得到的非线性误差的小波变换结果为  $e_{i'} = \Psi Y(s_{i'}) (i' = 1, 2)$ ,不同尺度对应的非线性误差相位为  $\varphi_{i'j} = \Psi \sin[j\varphi(u, s_{i'})]$  ( $j$  为非线性误差的谐波阶次),得到

$$\begin{bmatrix} A_1 \\ A_2 \end{bmatrix} = \begin{bmatrix} \varphi_{11} & \varphi_{12} \\ \varphi_{21} & \varphi_{22} \end{bmatrix}^{-1} \begin{bmatrix} e_1 \\ e_2 \end{bmatrix}. \quad (7)$$

重构一次谐波非线性误差函数为

$$E_{1\text{nonl}} = A_1 \sin[\varphi(u, s_1)]. \quad (8)$$

## 2.2 基于最小二乘非线性拟合函数的二次谐波非线性误差补偿

在补偿一次谐波非线性误差之后,采用基于最小二乘的非线性拟合方法对非线性二次谐波进行进一步补偿。根据实际实验测量可以得到二次谐波非线性误差曲线  $E_{2\text{nonl}}(x_i, y_i)$ ,基于最小二乘原理迭代,设定曲线拟合函数  $F(\alpha; x_{\text{data}})$  ( $x_{\text{data}}$  为自变量),使得拟合出的因变量  $y_{\text{data}}$  与实际的因变量  $y$  最为接近,则非线性最小二乘拟合的目标函数  $Q$  为

$$Q = \min_{\alpha} \|F(\alpha; x_{\text{data}}) - y_{\text{data}}\|_2^2 = \min_{\alpha} \sum_i [E_{2\text{nonl}}(\alpha; x_i) - y_i]^2, \quad (9)$$

式中:  $\alpha$  为待拟合曲线的参数,同时也是需要求解的对

象;  $E_{2\text{nonl}}(\alpha; x_i)$  为二次谐波非线性误差曲线;  $x_i$  为二次谐波非线性误差曲线对应的时间参数;  $y_i$  为二次谐波非线性误差曲线对应的误差值;  $i = 1, 2, 3$ 。等式左侧  $\|F(\alpha; x_{\text{data}}) - y_{\text{data}}\|_2^2$  表示求  $F(\alpha; x_{\text{data}}) - y_{\text{data}}$  二范数的平方, 即模长的平方。

迭代求最合适的  $\alpha$ , 由此得到二次谐波非线性误差拟合数据:

$$F = \begin{bmatrix} x_{\text{data}1} & F(\alpha; x_{\text{data}1}) \\ x_{\text{data}2} & F(\alpha; x_{\text{data}2}) \\ \vdots & \vdots \\ x_{\text{data}n} & F(\alpha; x_{\text{data}n}) \end{bmatrix}, \quad (10)$$

式中:  $x_{\text{data}n}$  为被拟合的二次谐波非线性误差曲线第  $n$  个点对应的的时间参数;  $n$  为非线性误差函数的数据点个数。

### 3 实 验

实验原理框图和实验装置如图 3 所示。双频激光器为哈尔滨超精密装备工程技术中心有限公司研制的 UOI-1500, 出射激光波长为 632 nm, 激光出光功率为

1.3 mW。1 级标准量块被放置在位移平台上。使用频谱仪采集干涉信号频谱。双频激光经过分光镜 (BS) 后, 一路经过偏振片 ( $P_1$ ) 到达光电接收器 ( $PD_1$ ), 这路光作为干涉测量的参考信号。另一路透射经过偏振分光镜 (PBS) 后分成两路: 初始 P 光透射经过四分之一波片 ( $QW_2$ ), 被标准量块反射再次经过  $QW_2$ , 此时最初的 P 光已经变成 S 光, S 光被 PBS 分束膜反射到角锥棱镜上, 反射光再次被 PBS 反射, 先后经过  $QW_2$ 、量块和  $QW_2$ , 光束再次变回 P 光, 经 PBS 透射; 初始 S 光被反射后经过四分之一波片 ( $QW_1$ ), 被参考镜 ( $M_1$ ) 反射后再次经过  $QW_1$ , 最初的 S 光变成 P 光, 经过 PBS 分束膜后透射到角锥棱镜上, 反射光再次经过 PBS 透射, 先后经  $QW_1$ 、参考镜  $M_1$  和  $QW_1$ , 光束再次变回 S 光, 经 PBS 反射。此时, 测量臂和参考臂合束被分光镜 BS 反射的部分经过偏振片到达光电接收器 ( $PD_2$ ), 这路光作为测量信号。通过处理测量信号和参考信号实现位移测量。将光电接收器  $PD_2$  输出的测量信号直接接入频谱仪, 对此光路的非线性误差进行测量。

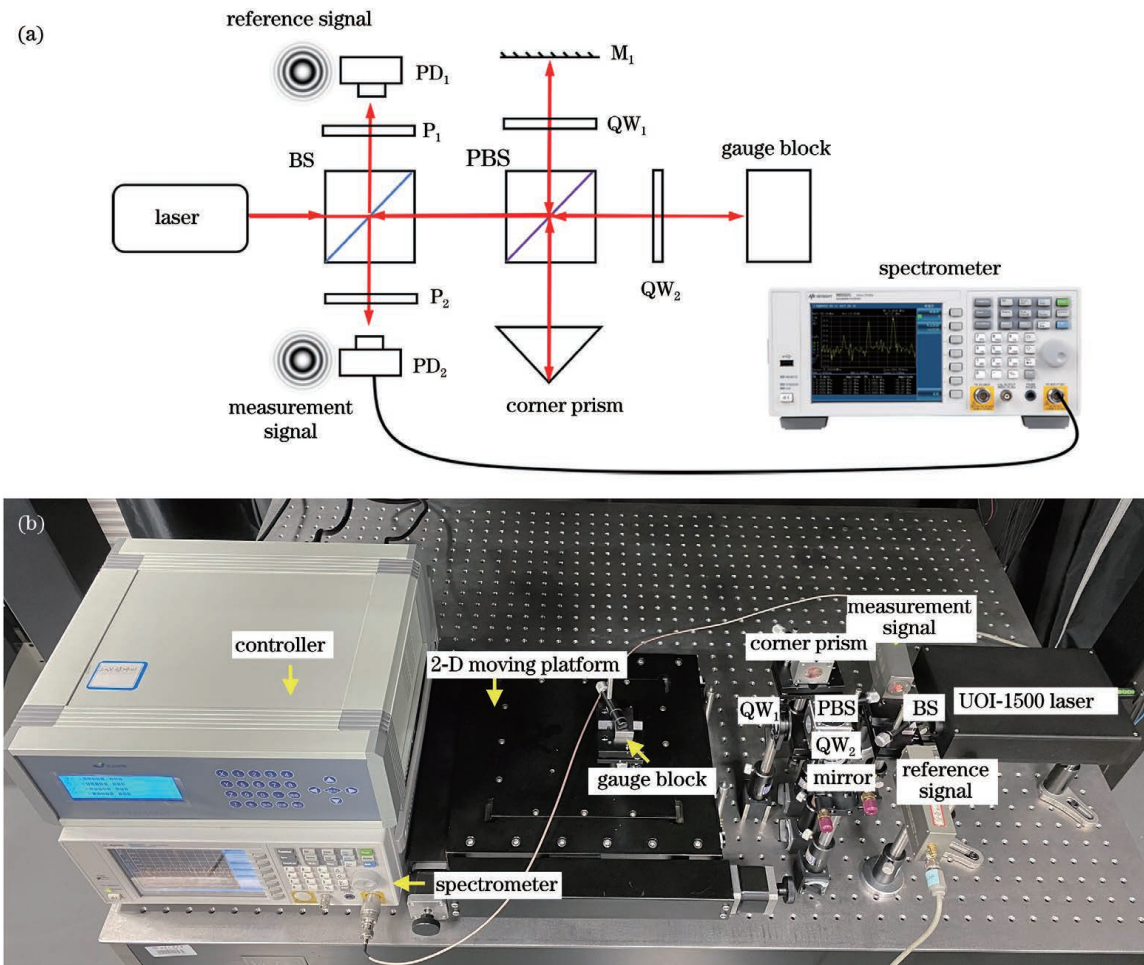


图 3 实验装置。(a) 原理图; (b) 实物图

Fig. 3 Experimental devices. (a) Schematic; (b) physical picture

当量块以 8 mm/s 的速度匀速运动时, 干涉信号频谱如图 4 所示。

非线性误差一次谐波幅值与测量信号幅值的比值  $\Delta_1$  为 6.51 dB, 非线性误差二次谐波幅值与测量信号

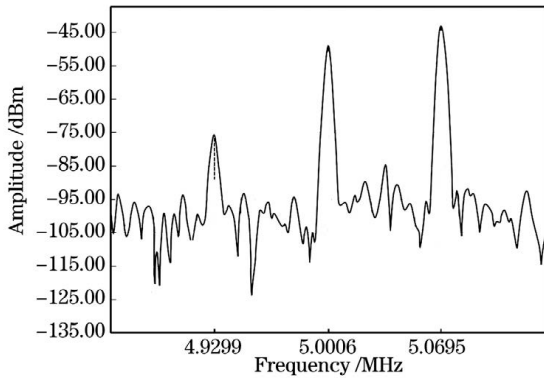


图 4 量块以 8 mm/s 的速度运动时的干涉信号频谱  
Fig. 4 Spectrum diagram of interference signal when gauge block moves at 8 mm/s

幅值的比值 $\Delta_2$ 为 34.2 dB, 得到非线性误差一次谐波和二次谐波的大小分别为 5.97 nm 和 0.25 nm。

利用本文提出的基于连续小波变换的激光外差干涉非线性误差补偿方法对非线性误差进行补偿。图 5 为非线性误差补偿前后的结果对比。测量系统的非线性误差分量由 5.97 nm 减小到 1.09 nm, 非线性误差分量减小至原来的 18%。

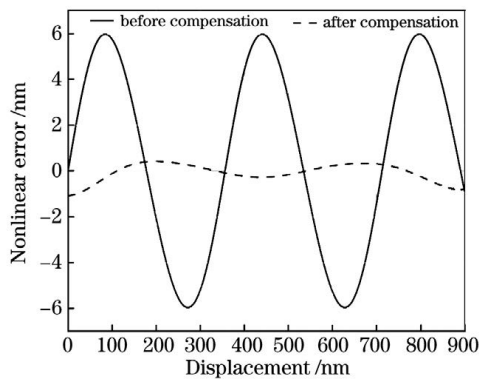


图 5 补偿前后的非线性误差

Fig. 5 Nonlinear errors before and after compensation

## 4 结 论

针对激光外差干涉测量中周期性非线性误差补偿问题, 提出了一种基于连续小波变换的激光外差干涉非线性误差补偿方法, 通过对非线性误差函数进行连续小波变换, 重构一次谐波非线性误差, 利用最小二乘非线性拟合方法迭代拟合出二次谐波非线性误差。实验结果表明: 将此方法应用于激光外差干涉测量系统中, 非线性误差分量由 5.97 nm 减小到 1.09 nm, 非线性误差分量减小至原来的 18%, 验证了所提方法的可行性。

## 参 考 文 献

- [1] Quenelle R. Nonlinearity in interferometric measurements[J]. Hewlett-Packard Journal, 1983, 34(4): 10.
- [2] 贾文昕, 韩森, 张凌华, 等. 离轴椭圆柱面镜测量方法及调整误差分析[J]. 光学学报, 2021, 41(20): 2012004.
- [3] Jia W X, Han S, Zhang L H, et al. Measurement method and alignment error analysis of off-axis elliptical cylindrical mirror[J]. Acta Optica Sinica, 2021, 41(20): 2012004.
- [4] Guo J H, Zhang Y, Shen S. Compensation of nonlinearity in a new optical heterodyne interferometer with doubled measurement resolution[J]. Optics Communications, 2000, 184(1/2/3/4): 49-55.
- [5] 陈洪芳, 钟志, 丁雪梅. 激光外差干涉的非线性误差补偿[J]. 光学精密工程, 2010, 18(5): 1043-1047.
- [6] Chen H F, Zhong Z, Ding X M. Compensation of nonlinear errors in laser heterodyne interferometers[J]. Optics and Precision Engineering, 2010, 18(5): 1043-1047.
- [7] Chen H F, Jiang B, Shi Z Y. Synthetic model of nonlinearity errors in laser heterodyne interferometry[J]. Applied Optics, 2018, 57(14): 3890-3901.
- [8] Fu H J, Hu P C, Tan J B, et al. Simple method for reducing the first-order optical nonlinearity in a heterodyne laser interferometer[J]. Applied Optics, 2015, 54(20): 6321-6326.
- [9] Lu Z G, Zhang Y L, Liang Y T, et al. Measuring the laser polarization state and PBS transmission coefficients in a heterodyne laser interferometer[J]. IEEE Transactions on Instrumentation and Measurement, 2018, 67(3): 706-714.
- [10] Yang Y, Deng Y, Tan Y D, et al. Nonlinear error analysis and experimental measurement of Birefringence-Zeeman dual-frequency laser interferometer[J]. Optics Communications, 2019, 436: 264-268.
- [11] 谈宜东, 徐欣, 张书练. 激光干涉精密测量与应用[J]. 中国激光, 2021, 48(15): 1504001.
- [12] Tan Y D, Xu X, Zhang S L. Precision measurement and applications of laser interferometry[J]. Chinese Journal of Lasers, 2021, 48(15): 1504001.
- [13] Eom T B, Choi T Y, Lee K H, et al. A simple method for the compensation of the nonlinearity in the heterodyne interferometer[J]. Measurement Science and Technology, 2002, 13(2): 222-225.
- [14] Eom T B, Kim J A, Kang C S, et al. A simple phase-encoding electronics for reducing the nonlinearity error of a heterodyne interferometer[J]. Measurement Science and Technology, 2008, 19(7): 075302.
- [15] Wang C, Burnham-Fay E D, Ellis J D. Real-time FPGA-based Kalman filter for constant and non-constant velocity periodic error correction[J]. Precision Engineering, 2017, 48: 133-143.
- [16] 严利平, 周春宇, 谢建东, 等. 基于卡尔曼滤波的 PGC 解调非线性误差补偿方法[J]. 中国激光, 2020, 47(9): 0904002.
- [17] Yan L P, Zhou C Y, Xie J D, et al. Nonlinear error compensation method for PGC demodulation based on Kalman filtering[J]. Chinese Journal of Lasers, 2020, 47(9): 0904002.
- [18] Lawall J, Kessler E. Michelson interferometry with 10 pm accuracy[J]. Review of Scientific Instruments, 2000, 71(7): 2669-2676.
- [19] Fu H J, Wang Y, Ji R D, et al. A real-time nonlinear error measurement method with picometer accuracy and free from target motion state[J]. Proceedings of SPIE, 2019, 11053: 899-904.
- [20] Fu H J, Wang Y, Hu P C, et al. Nonlinear errors resulting from ghost reflection and its coupling with optical mixing in heterodyne laser interferometers[J]. Sensors, 2018, 18(3): 758.
- [21] 王越, 胡鹏程, 付海金, 等. 外差激光干涉仪周期非线性误差形成机理与补偿方法[J]. 哈尔滨工业大学学报, 2020, 52(6): 126-133.
- [22] Wang Y, Hu P C, Fu H J, et al. Periodic nonlinear error and its compensation method in heterodyne laser interferometer[J]. Journal of Harbin Institute of Technology, 2020, 52(6): 126-133.
- [23] 郝义伟, 孔新新, 才啟胜, 等. 环形器噪声对激光干涉测量系统影响分析[J]. 光学学报, 2021, 41(9): 0912003.
- [24] Hao Y W, Kong X X, Cai Q S, et al. Analysis of effect of circulator noise on laser interferometry system[J]. Acta Optica Sinica, 2021, 41(9): 0912003.

[19] Yu X, Lai S S, Liu Y K, et al. Generic nonlinear error compensation algorithm for phase measuring profilometry [J]. Chinese Optics Letters, 2021, 19(10): 101201.

[20] Lu C, Troutman J R, Schmitz T L, et al. Application of the continuous wavelet transform in periodic error compensation [J]. Precision Engineering, 2016, 44: 245-251.

## Nonlinear Error Compensation Method for Laser Heterodyne Interferometry Based on Continuous Wavelet Transform

Wang Yu, Chen Hongfang\*

<sup>1</sup>Beijing Engineering Research Center of Precision Measurement Technology and Instruments, Department of Materials and Manufacturing, Beijing University of Technology, Beijing 100124, China

### Abstract

**Objective** The development trend of laser heterodyne interferometry is the enhancement of measurement resolution and accuracy. The primary factor that hinders the further enhancement of laser heterodyne interferometry accuracy is the periodic nonlinear error. This research proposes a nonlinear error compensation approach for laser heterodyne interferometry based on wavelet transform. The Morlet wavelet transform is employed for the nonlinear error function, and the wavelet ridge is extracted from the wavelet coefficient matrix's information. Next, the characteristic information of wavelet ridge line is examined and the first harmonic nonlinear error is rebuilt. After compensating for the first harmonic nonlinear error based on the wavelet transform approach, the second harmonic nonlinear error is fitted iteratively by the least-squares nonlinear fitting approach.

**Methods** First, a nonlinear error compensation approach based on a wavelet transform is proposed. Periodic nonlinear errors in laser heterodyne interference systems can be modeled as the superposition of pure sine waves. The wavelet family is created by changing the time and scale factors of complex Morlet wavelet. The pure sinusoidal model is converted using wavelet transform based on the Morlet wavelet family. By further computation, the wavelet coefficient's modulus and phase are obtained, so that the wavelet ridge is extracted. When the modulus of the wavelet system is the largest at the ridge position, the corresponding scale corresponds to the first harmonic nonlinear error frequency. The first harmonic nonlinear error phase is the corresponding phase. The second harmonic nonlinear error frequency is twice that of the first harmonic nonlinear error. Additionally, the second harmonic nonlinear error phase is achieved under the corresponding frequency's scale. Based on this, the first harmonic nonlinear error function's amplitude is computed, and the rebuilt first harmonic nonlinear error function model is achieved. After compensating for the first harmonic nonlinear error, the nonlinear fitting approach based on the least square is employed to further fit the nonlinear second harmonic. Furthermore, a laser heterodyne interferometer optical path is constructed to measure nonlinear errors. The nonlinear error compensation based on the wavelet transform is employed for the nonlinear error measurement, and the actual compensation impact is investigated.

**Results and Discussions** Based on the principle of laser heterodyne interference, an experimental optical path of laser heterodyne interference is constructed (Fig. 3). The measurement signal's nonlinear error in the experimental device is measured. The interference signal's spectrum when the gauge block moves at 8 mm/s is examined (Fig. 4). The first harmonic's magnitude and the nonlinear error's second harmonic are 5.97 nm and 0.25 nm, respectively. The nonlinear error compensation approach for laser heterodyne interference based on the continuous wavelet transform is employed to compensate for the nonlinear error. The measurement system's nonlinear error component decreases from 5.97 nm to 1.09 nm, and the nonlinear error component is reduced to 18% of the original. Based on this approach, the impact of nonlinear error can be suppressed efficiently and the measurement accuracy of laser heterodyne interference can be enhanced.

**Conclusions** By addressing the challenge of periodic nonlinear error compensation in laser heterodyne interferometry, a nonlinear error compensation approach based on continuous wavelet transform is proposed. The Morlet wavelet transform is employed for the nonlinear error function, and the wavelet ridge is extracted from the wavelet coefficient matrix's information. Next, the characteristic information of wavelet ridge line is examined and the first harmonic nonlinear error is rebuilt. After compensating for the first harmonic nonlinear error based on the wavelet transform approach, the second harmonic nonlinear error is fitted iteratively using the least-squares nonlinear fitting approach. Experimental findings demonstrate that the nonlinear error component decreases from 5.97 nm to 1.09 nm, and the nonlinear error component

is reduced to 18% of the original when the approach is employed for laser heterodyne interferometry. Based on this approach, the impact of nonlinear errors can be suppressed efficiently and the measurement accuracy of laser heterodyne interference can be enhanced.

**Key words** measurement; laser heterodyne interferometry; nonlinear error; continuous wavelet transform; least-squares nonlinear fitting